EurJIC European Journal of Inorganic Chemistry
ChemPubSoc Europe
FULL PAPER

DOI:10.1002/ejic.201402918

Synthesis and Characterization of Bio-Inspired Diiron Complexes and Their Catalytic Activity for Direct Hydroxylation of Aromatic Compounds

Xiao Wang,[a,b] Tianyong Zhang,*[a,b] Qiusheng Yang,[c] Shuang Jiang,[a,b] and Bin Li*[a,b]

Keywords: Diiron complex / Hydroxylation / Aromatic compounds / O–O activation / Density functional calculations

Three [FeFe]-hydrogenase model complexes [(μ-dmedt)-{Fe(CO)$_3$}$_2$] [**1**; dmedt = SCH(CH$_3$)CH(CH$_3$)S], [(μ-dmedt)-{Fe(CO)$_3$}{Fe (CO)$_2$PPh$_3$}] (**1**-PPh$_3$), and [(μ-dmest)-{Fe(CO)$_3$}$_2$] [**1**-O; dmest = SCH(CH$_3$)CH(CH$_3$)S(O)], **1**-O were synthesized and characterized. These model complexes, which are generally used as the functional biomimics of the hydrogen-producing dinuclear active site in [FeFe]-hydrogenase, were used as efficient catalysts for the selective hydroxylation of aromatic compounds to phenols under mild conditions. Because both the dithiolato-sulfur site and the Fe–Fe bond in the model complexes were possible active oxidation sites, DFT calculations were used to investigate the oxygenated products, that is, the S-oxygenated products or the Fe-oxygenated forms of the model complexes, which may be involved in the catalytic cycle. The experimental and computational results indicate that the thermodynamically favored Fe-oxygenated intermediates dominate the hydroxylation of the aromatic compounds. A possible mechanism for the hydroxylation is also proposed.

Introduction

The direct catalytic hydroxylation of aromatic compounds to phenols under mild conditions remains a major challenge in industrial and synthetic chemistry[1–5] and has attracted considerable interest, the ultimate goal of which is to find a substitute for the multistep and environmentally hazardous process used today.[6] Among various catalysts for the selective hydroxylation of aromatic compounds, iron-based catalysts have been an active research area for many years,[7–10] because they catalyze a number of chemically challenging oxidative processes with high selectivity and reaction rates,[11,12] and because iron is geologically abundant. Especially, iron-based biomimetic catalysts with accessible redox states for selective oxygen binding and activation are studied to mimic the monoiron or diiron sites of the natural oxygenase enzymes (cytochrome P450, methane monooxygenases, etc.) and were used as efficient catalysts for selective hydrocarbon oxidation.[13–15] The catalytic activities of these iron-based biomimetic catalysts have been investigated,[16–19] and some mechanistic guidelines for the understanding of the iron-centered aromatic hydroxylation have been summarized.[20,21] Environmentally friendly oxidants, such as H_2O_2[22–24] and O_2,[25–27] are usually used in the selective hydroxylation of inert aromatic compounds.

Recently, research on the [FeFe]-hydrogenases and their model complexes, which are much more efficient in the H_2 production compared to other types of hydrogenases, has attracted much attention.[28–33] However, the well-known oxygen sensitivity of the hydrogenases and their active-site biomimetics poses a problem for their development as alternatives to platinum in fuel cell applications. As reported, the oxygenation of the diiron (Fe^I–Fe^I, Fe^I–Fe^{II}, and Fe^{II}–Fe^{II}) organometallics that model the diiron subsite in the active site of [FeFe]-hydrogenase enzymes would occur at the dithiolato-sulfur site or at the Fe–Fe bond.[34,35] This would lead to either the S-oxygenated products, in which the oxygen atom is relatively stable, or the Fe-oxygenated products (Fe^{II}–μ-O–Fe^{II} oxidative addition products), which are thermodynamically favored but not detected in the oxygenation reaction. According to the theoretical calculations, the diiron Fe^I–Fe^I subsite is thermodynamically favored to be oxidized to the Fe^{II}–μ-O–Fe^{II} species. Because the highly active (μ-oxido)diiron derivatives are accepted as the crucial intermediates that transfer oxygen in the biomimetic hydrocarbon hydroxylation,[36–39] we propose that the

[a] Tianjin Key Laboratory of Applied Catalysis Science and Technology, School of Chemical Engineering and Technology, Tianjin University,
Tianjin 300072, P. R. China
E-mail: tyzhang@tju.edu.cn
libin@tju.edu.cn
http://chemeng.tju.edu.cn/
[b] Collaborative Innovation Center of Chemical Science and Engineering,
Tianjin 300072, P. R. China
[c] School of Chemical Engineering and Technology, Hebei University of Technology,
Tianjin 300130, China
Supporting information for this article is available on the WWW under http://dx.doi.org/10.1002/ejic.201402918.

active Fe^{II}–μ-O–Fe^{II} species formed by the oxidation of the [FeFe]-hydrogenase model complex may be a potential oxygen-transfer intermediate in the presence of an oxygen-atom moderator such as the aromatic compound.

In this study, three [FeFe]-hydrogenase model complexes were synthesized (Figure 1) and applied in the catalytic oxidation of aromatic hydrocarbons with high selectivity. The catalytic activity of these model complexes and DFT calculations provided effective verification that the Fe-oxygenated forms of the diiron complexes were responsible for the hydroxylation.

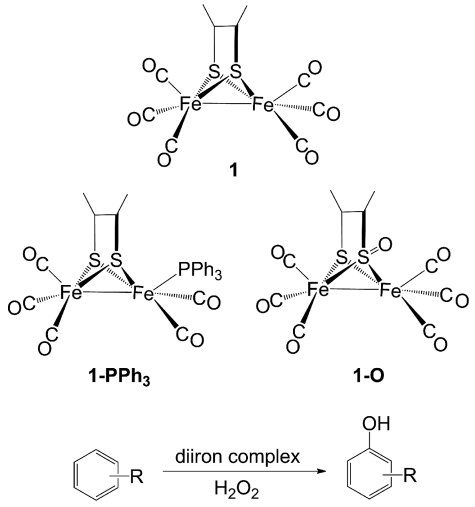

Figure 1. Structures of the [FeFe]-hydrogenase model complexes, and hydroxylation of aromatic compounds.

Results and Discussion

Characteristics of the Diiron Complexes

The IR spectroscopic data in the CO-stretching-vibration region of the complexes were recorded with hexane solutions of the complexes, as shown in Figure 2. The IR pattern of **1** is similar to that of the typical diiron complex [(μ-pdt){$Fe(CO)_3$}$_2$]. However, because of the different electronic and steric effects of the S–S linker, the ν̃ (CO) bands of **1** appear at slightly higher wavenumbers.[40] In comparison to **1**, the complex **1**-PPh_3 exhibits ν̃(CO) bands at lower wavenumbers, and the positions of the bands depend on the donor abilities of the ligand PPh_3. The ν̃(CO) bands of **1**-O are at higher wavenumbers because of the electron-withdrawing oxygen atom attached to one sulfur atom.

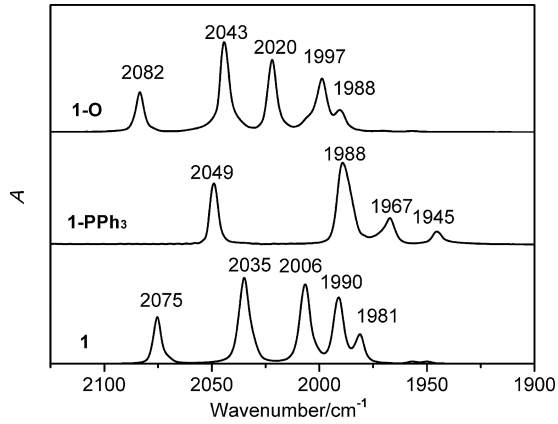

Figure 2. The ν̃(CO) region of IR spectra of complexes **1**, **1**-PPh_3, and **1**-O (observed in hexane solution).

The molecular structures of the complexes are shown in Figure 3. Selected bond lengths and bond angles are listed in Table 1, and the crystallographic data are listed in Table S1. The central 2Fe2S cores of the complexes are all

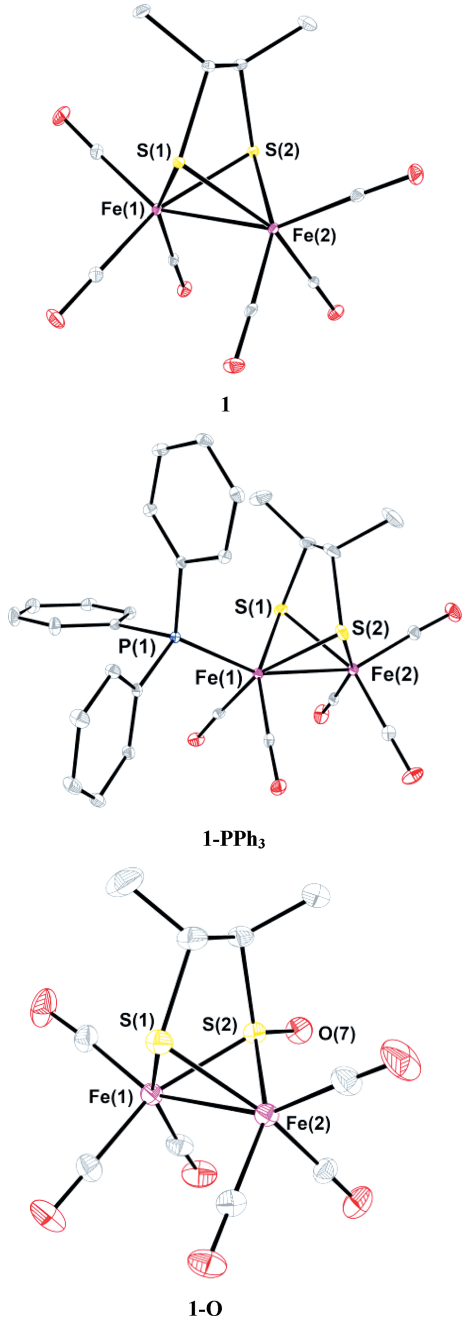

Figure 3. Crystal structures of the complexes (ellipsoids are drawn at the 30% probability level). Hydrogen atoms are omitted for clarity.

in the butterfly conformation similar to the previously reported models,[41–43] and the iron atom is coordinated in a pseudo-square-pyramidal geometry. The substitution of CO by one PPh_3 ligand only has a small effect on the Fe–Fe distance, and the PPh_3 ligand is coordinated to an apical site on Fe(1), and it is positioned roughly *trans* to the Fe–Fe bond. The coordinative configuration of **1**-O is essentially identical to that of **1**. As a result of the oxygenation of one dithiolato sulfur atom, a shorter Fe–S bond and a longer Fe–Fe bond are observed in **1**-O.

Table 1. Selected bond lengths [Å] and bond angles [°] of **1**, **1**-PPh_3, and **1**-O.

	1	**1**-PPh_3	**1**-O
Fe(1)–Fe(2)	2.5091(8)	2.5149(7)	2.5356(10)
Fe(1)–S(1)	2.2522(6)	2.2464(8)	2.1763(11)
Fe(1)–S(2)	2.2398(7)	2.2589(11)	2.2456(14)
Fe(2)–S(1)	2.2507(7)	2.2637(8)	2.1774(13)
Fe(2)–S(2)	2.2468(6)	2.2510(8)	2.2457(13)
Fe(1)–P(1)	–	2.2535(8)	–
S(2)–O(7)	–	–	1.474(3)
S(1)–Fe(1)–Fe(2)	56.109(14)	56.44(2)	55.40(4)
S(1)–Fe(2)–Fe(1)	56.16(2)	55.78(2)	54.36(3)
S(2)–Fe(1)–Fe(2)	56.13(2)	55.96(3)	55.63(4)
S(2)–Fe(2)–Fe(1)	55.86(2)	56.23(3)	55.63(4)
P(1)–Fe(1)–Fe(2)	–	156.80(2)	–
O(7)–S(2)–Fe(2)	–	–	109.20(17)

Electrochemistry

The redox properties of **1**, **1**-PPh_3, and **1**-O were studied by cyclic voltammetry (Figure 4). The electrochemical data are given in Table 2. On the basis of previous reports on [(μ-pdt){$Fe(CO)_3$}$_2$], the cyclic voltammogram (CV) of **1** displays a quasi-reversible reduction event at E_{pc} = –1.72 V, an irreversible reduction process at E_{pc} = –2.21 V, and an irreversible oxidation process at E_{pa} = +0.98 V. The first reduction event can be assigned to the Fe^IFe^I/Fe^IFe^0 reduction, the second reduction event can be assigned to the Fe^IFe^0/Fe^0Fe^0 reduction, and the oxidation process can be assigned to the $Fe^IFe^I/Fe^{II}Fe^I$ oxidation.[44,45] The CV of the PPh_3-substituted complex **1**-PPh_3 in CH_3CN displays one irreversible reduction event (Fe^IFe^I/Fe^IFe^0) at E_{pc} = –1.91 V, a quasi-reversible reduction event (Fe^IFe^0/Fe^0Fe^0) at E_{pc} = –2.22 V and two irreversible oxidation events at E_{pa} = +0.51 and +1.02 V. The second irreversible oxidation event of **1**-PPh_3 at approximately +1.02 V is tentatively assigned to the $Fe^{II}Fe^I/Fe^{II}Fe^{II}$ oxidation. The electrochemical data for **1**-PPh_3 show cathodic shifts of approximately 190 mV for the Fe^IFe^I/Fe^IFe^0 reduction, as compared to the all-CO complex **1**, and this is consistent with the fact that CO has been exchanged for a more electron-donating ligand. For **1**-PPh_3, the event presumed to be a $Fe^IFe^I/Fe^{II}Fe^I$ oxidation becomes more accessible by approximately 470 mV, as compared to **1**. According to the related literature, these redox events are all one-electron processes.[46,47] In addition to the quasi-reversible reduction event at E_{pc} = –1.57 V, complex **1**-O displays a second irreversible reduction event at E_{pc} = –2.35 V. For the S-oxygenated complex **1**-O, the irreversible oxidation event presumed to be a $Fe^IFe^I/Fe^{II}Fe^I$ process has become more anodic by approximately 190 mV, as compared to **1**, which is consistent with the electron-withdrawing ability of the oxygen atom attached to the dithiolato sulfur atom. For **1**-O, the reduction potential at –1.72 V is identical to that of the Fe^IFe^I/Fe^IFe^0 couple of complex **1**, which implied that some deoxygenation process of **1**-O produced the precursor dithiolate **1** as demonstrated in a previous report for [(μ-pdt){$Fe(CO)_3$}$_2$].[34]

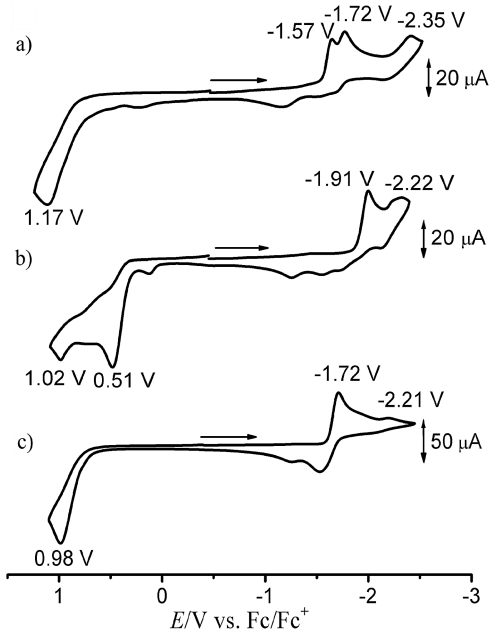

Figure 4. Cyclic voltammograms of the diiron complexes (2.0 mM) in CH_3CN solution (0.1 M nBu_4NPF_6; scan rate 50 mV/s): (a) **1**-O, (b) **1**-PPh_3, and (c) **1**.

Table 2. Redox potentials of the complexes.

	*E*pc [V] vs. Fc/Fc^+	*E*pa [V] vs. Fc/Fc^+
	E_1: $Fe^IFe^I \rightarrow Fe^IFe^0$ E_2: $Fe^IFe^0 \rightarrow Fe^0Fe^0$	$Fe^IFe^I \rightarrow Fe^{II}Fe^I$ $Fe^{II}Fe^I \rightarrow Fe^{II}Fe^{II}$
1	–1.72	0.98
	–2.21	–
1-PPh_3	–1.91	0.51
	–2.22	1.02
1-O	–1.57	1.17
	–2.35	–

Hydroxylation of Aromatic Compounds

As diiron complexes are well known for catalyzing hydrocarbon oxidation and the [FeFe]-hydrogenase model complexes are typical diiron carbonyl complexes, the model complex **1** was applied as a catalyst for the direct hydroxylation of benzene to phenol, to investigate whether the model complexes are capable of transferring oxygen. A blank control experiment (without catalyst) was conducted, and no phenol was detected.

O_2, H_2O_2, iodosobenzene (PhIO), and *m*-chloroperoxybenzoic acid (*m*-CPBA) were used (Table 3) as oxidants in the hydroxylation catalysis. A higher phenol yield was observed with H_2O_2 than with *m*-CPBA under otherwise identical conditions. However, O_2 and PhIO were not able to oxidize benzene to phenol in the presence of the model complex under the given experimental conditions (see footnote in Table 3). Thus, H_2O_2 was used as the oxidant in the following hydroxylation experiments.

Table 3. Catalytic hydroxylation of benzene to phenol with different oxidants.[a]

Entry	Oxidant	Yield [%]	Selectivity[b] [%]
1	*m*-CPBA	3.4	93.2
2	O_2	0	0
3	H_2O_2	7.5	92.5
4	PhIO	0	0

[a] **1**, 0.05 mmol; 60 °C; benzene, 0.1 mL; CH_3CN, 2.0 mL; oxidants, 5.0 mmol; reaction time, 3 h. [b] Selectivity: yield of phenol/benzene conversion.

Some parameters that affected the catalytic activity of the catalyst, such as the amount of H_2O_2, the temperature, and the reaction time, were also investigated. The phenol yield is greatly influenced by the amount of H_2O_2 (Table 4). Initially, it increases with added increments of H_2O_2, and it then decreases as a result of overoxidation of phenol to other by-products (dihydroxybenzenes, benzoquinone) with excess H_2O_2. The phenol yield and selectivity are plotted as a function of temperature in Figure 5. No product is detected below 40 °C, because a longer induction period at low temperatures prevents the formation of phenol. The selectivity decreases with an increase of temperature, and this is attributed to the accelerated overoxidation of phenol. As illustrated in Figure 6, the phenol yield reaches a maximum after 3 h. Decreased selectivity as a result of phenol overoxidation is also observed upon prolonging the reaction time. Under the optimized experimental conditions (**1**, 0.05 mmol; 60 °C; benzene, 0.1 mL; CH_3CN, 2.0 mL; H_2O_2, 5.0 mmol; reaction time, 3 h), the phenol yield is 7.5% with 92.5% selectivity.

Table 4. Effects of the H_2O_2 amount on the phenol yield in the hydroxylation of benzene.[a]

Entry	H_2O_2 [mmol]	Yield [%]	Selectivity [%]
1	1.0	2.7	96.4
2	3.0	4.9	93.1
3	5.0	7.5	92.5
4	8.0	5.4	87.2

[a] **1**, 0.05 mmol; 60 °C; benzene, 0.1 mL; CH_3CN, 2.0 mL; H_2O_2; reaction time, 3 h.

Additionally, **1** can catalyze the hydroxylation of a series of aromatic compounds to the corresponding phenols with high selectivity as well, which reveals the good substrate adaptability (Table 5) of the catalytic system.

According to previous results, the diiron model complexes could undergo a nucleophilic attack at both the metal center and the bridging thiolate sulfur atom.[48–50] Liu et al.[34] investigated whether the O-atom addition to [(μ-pdt){Fe(CO)$_2$L}$_2$] might provide examples of both S-site and metal-site reactivity. Treatment of [(μ-pdt){Fe(CO)$_2$-P(Me)$_3$}$_2$] with *m*-CPBA led to decomposition and the formation of a mononuclear iron(II) complex, which pointed to a Fe-based oxidation. They also observed that the [FeFe]-hydrogenase model complexes could perform sulfur-based oxygenation, which is consistent with earlier literature reports.[51–53] Thus, oxygenation of the [FeFe]-hydrogenase model complex may occur at the dithiolato sulfur site or the Fe–Fe site. Because the catalysts should first be oxidized by the oxidants before they enter the catalytic cycle, both the S-oxygenated products and Fe-oxygen-

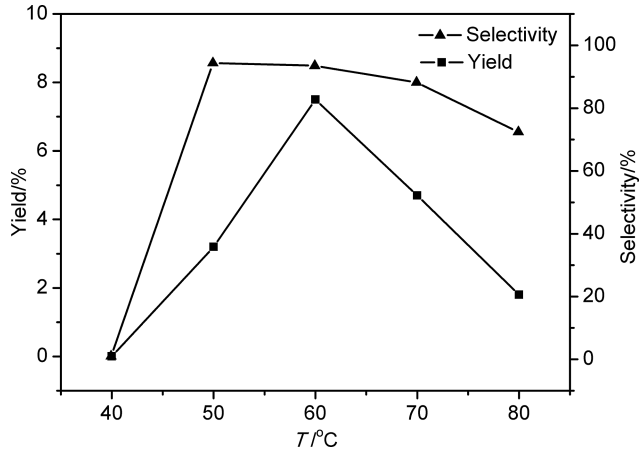

Figure 5. Effects of the reaction temperature on the phenol yield in the hydroxylation of benzene (**1**, 0.05 mmol; benzene, 0.1 mL; CH_3CN, 2.0 mL; H_2O_2, 5.0 mmol; reaction time, 3 h).

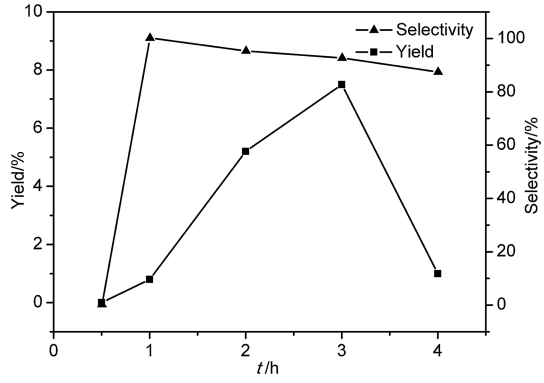

Figure 6. Effects of the reaction time on the phenol yield in the hydroxylation of benzene (**1**, 0.05 mmol; 60 °C; benzene, 0.1 mL; CH_3CN, 2.0 mL; H_2O_2, 5.0 mmol).

Table 5. Hydroxylation of different substrates catalyzed by **1**.[a]

Entry	Substrate	Product (yield [%])	Selectivity [%]
1	phenol	hydroquinone (17.4)	86.7
2	*p*-xylene	2,5-xylenol (14.5)	90.5
3	naphthalene	1-naphthol (9.2)	92.4
4	chlorobenzene	*p*-chlorophenol (1.5)	95.2

[a] **1**, 0.05 mmol; 60 °C; molar ratio of substrate to H_2O_2 is 1:5; CH_3CN, 2.0 mL; reaction time, 3 h.

ated forms of the model complexes may have the potential to transfer oxygen atoms in the hydroxylation.

When **1**-O was used as the catalyst, phenol was detected (Table 6). In this case, the oxidant H_2O_2 could only attack the Fe–Fe bond, because the S(O) site in **1**-O is relatively stable and not able to release the oxygen atom. Thus, we speculated that the oxygenation of the Fe–Fe bond might be part of the hydroxylation cycle. Furthermore, the complexes **1**, **1**-O, and **1**-PPh_3 could all catalyze the hydroxylation of benzene, and their activity decreases in the order **1**-PPh_3 > **1** > **1**-O under identical conditions (Table 6). The different activities of **1**, **1**-PPh_3, and **1**-O originate from the different Fe–Fe electron densities of these model complexes. The Fe–Fe bond in the complex with the electron-donating PPh_3 ligand could be oxidized more easily by H_2O_2 to form the oxygen-transfer intermediate, whereas the less electron-rich complexes tended to be less reactive with this oxidant.

Table 6. Effects of different catalysts on the phenol yield in the hydroxylation of benzene.[a]

Entry	Catalyst	Yield [%]	Selectivity [%]
1	**1**	7.5	92.5
2	**1**-PPh_3	9.6	93.3
3	**1**-O	3.7	95.6

[a] Catalyst, 0.05 mmol; 60 °C; benzene, 0.1 mL; CH_3CN, 2.0 mL; H_2O_2, 5.0 mmol; reaction time, 3 h.

As seen from the IR spectra (Figure 7), the wavenumbers of the CO-stretching bands of complex **1** had not changed after the hydroxylation, except for slightly decreased intensities. This indicates the structural preservation of the catalyst. The characteristic CO-stretching bands of complex **1**-O were not detected under the experimental conditions applied during catalysis. This implicates that complex **1** was not oxidized to **1**-O, in which only the Fe–Fe bond was reactive towards oxygenation. We thus conclude that the catalytic activity of the model complex derives from the Fe–Fe bond. Some decomposition of complex **1** can be deduced from the decreased intensities of the CO-stretching bands.

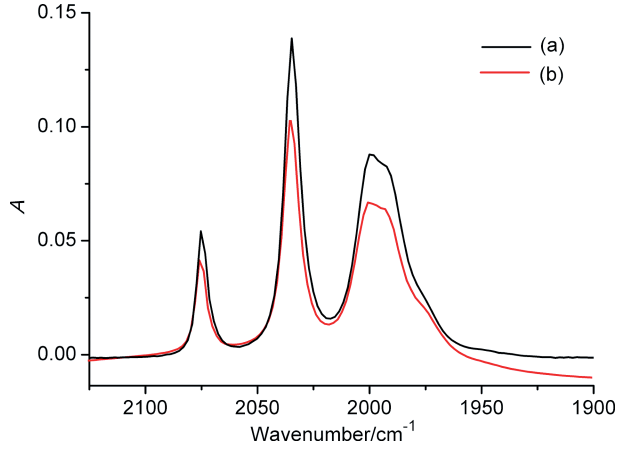

Figure 7. The ν̃(CO) region of IR spectra of (a) complex **1** and (b) complex **1** after benzene hydroxylation (recorded in CH_3CN solution).

Accordingly, Fe-based oxygenation dominates the hydroxylation cycle as concluded from the above experiments. However, which kind of Fe-oxygenated product is responsible for the catalytic activity is not evident from the catalytic hydroxylation experiments.

Theoretical Details

DFT calculations suggest that the Fe–Fe bond in [(μ-pdt){$Fe(CO)_3$}$_2$] or its derivatives is thermodynamically favored to be oxidized to the μ-oxido product Fe^{II}–μ-O–Fe^{II}. On the basis of these results and the above-mentioned conclusion that the hydroxylation reactivity of the diiron complexes stems from the oxygenation of the Fe–Fe bond, we assumed that the Fe^{II}–μ-O–Fe^{II} species is the potential oxygen-transfer species in the hydroxylation of aromatic compounds. Theoretical calculations similar to literature reports[34] were carried out to compare metal-based and sulfur-based oxygenation of the active-site paradigm of [(μ-dmedt){$Fe(CO)_3$}$_2$] (**1**), that is, to compare **1**-μ-O (Fe-based oxygenation product of **1**) and **1**-O (S-oxygenated product of **1**) with respect to the thermodynamic possibility of their formation.

To support our choice for the function and the basis set, the DFT calculations were performed for isolated complexes **1**, **1**-PPh_3, and **1**-O first, for which the experimental geometrical parameters are available in this article. The optimized geometrical parameters (Figures S1–S3, Tables S2–S7) are in good agreement with the experimental data obtained by X-ray diffraction analyses (deviations <5%), which confirms the reliability of the calculation method used for describing the present system.

As illustrated in Scheme 1, the difference of the total free energy (Δ*G*) between **1**-O and **1**-μ-O (Figure S4, Tables S8–S9) is 30.61 kcal/mol. Similarly, for all the model complexes, the μ-O isomeric form is calculated to be more thermodynamically favored for complexes **1**-PPh_3-μ-O-apical than for **1**-PPh_3-O-apicial, for **1**-PPh_3-μ-O-basal than for **1**-PPh_3-O-basal, and for **1**-O-μ-O than for **1**-O-O (Figures S5–S10, Tables S10–S21). The μ-O isomers are thermodynamically favored, as was reported for similar complexes [(μ-pdt){$Fe(CO)_2$L}{$Fe(CO)_2$L′}. In other words, the Fe–Fe bond in the diiron subsite is more susceptible to oxidation. The positional isomers of the S-oxygenated products and the μ-O complexes of **1**-PPh_3, that is, species that feature PPh_3 in apical or basal positions, have different Δ*G* values (ΔG_{2a} or ΔG_{2b}, respectively).

As illustrated in Figure 8, the HOMO of **1**, which is characterized by a large contribution of the Fe–Fe bond, also suggests that the Fe–Fe bond is active towards oxidation. In addition to the fact that the oxygen atom attached to the sulfur atom in the S-oxygenated product is relatively stable, one could speculate that the Fe^{II}–μ-O–Fe^{II} active intermediate is capable of transferring the oxygen atom to the aromatic substrates in the hydroxylation reaction.

The previous DFT results suggested that the Fe-based oxygenation of [(μ-pdt){$Fe(CO)_2$L}{$Fe(CO)_2$L′}] com-

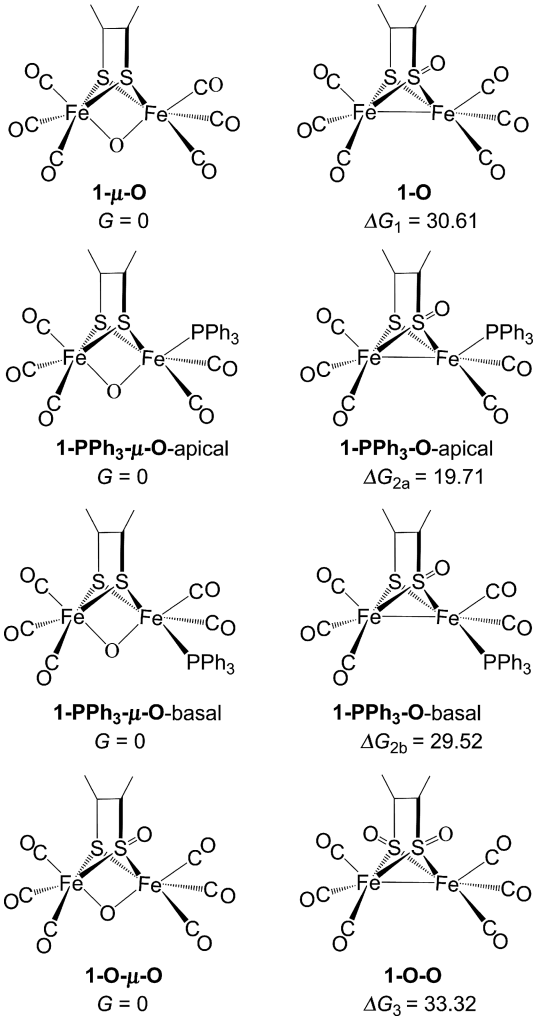

Scheme 1. Comparison of the total free energies [kcal/mol] of metal-oxygenated species and corresponding sulfur-oxygenated isomers. The values were obtained from computations with functionals and basis sets of B3LYP/D95 and LANL2DZ.

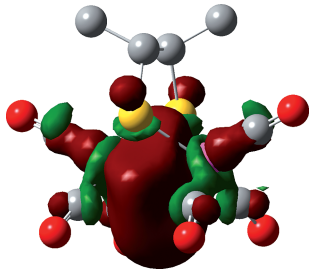

Figure 8. HOMO (isovalue: 0.02) of complex **1**.

plexes, which leads to Fe^{II}–μ-O–Fe^{II} species, was more thermodynamically favored than the S-based oxygenation. This implicates the possibility that the μ-O complex forms through Fe–Fe bond oxygenation in the [FeFe]-hydrogenase model complex. Unexpectedly, in previous reports, the thermodynamically favored Fe-oxygenated products were not observed when the model complexes were treated with oxidants.

To get the Fe-oxygenated product, that is, the complex **1**-μ-O, **1** was treated with different oxidants, such as *m*-CPBA, PhIO, O_2, and H_2O_2, in CH_3CN at room temperature, –10 °C, or –20 °C, and the reaction was monitored by IR spectroscopy. However, no obvious change of the CO-stretching-band wavenumbers was observed. The μ-O complex was not detected under the experimental conditions in the presence of the oxidants mentioned above. This may be attributed to the high activity of the transient iron–oxido species. Nevertheless, whether the μ-O complex was formed in the above reaction or not could not be determined. The hydroxylation of the aromatic compounds to the corresponding phenols catalyzed by the [FeFe]-hydrogenase model complexes offers an indirect evidence for the presence of a highly active Fe-oxygenated intermediate.

Proposed Mechanism of Hydroxylation

On the basis of the theoretical and experimental results, we propose a possible mechanism for the hydroxylation of the aromatic compounds (typically for the benzene hydroxylation). The nature of the phenol products resulting from the hydroxylation of different substrates catalyzed by the [FeFe]-hydrogenase model complex suggests that the reaction involves an electrophilic addition process, as illustrated in Scheme 2. Combined with the electrophilic addition process, a hydrogen-atom shift occurs.[54] In the last step, the oxygen atom is transferred to the substrates.

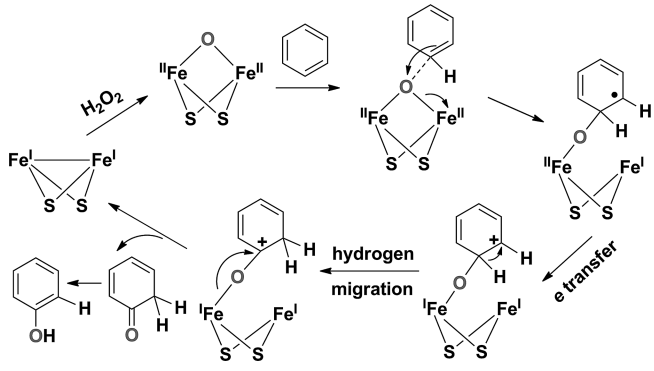

Scheme 2. Proposed mechanism for benzene hydroxylation.

Conclusions

In summary, we have synthesized and characterized three [FeFe]-hydrogenase model complexes and tested them as homogeneous catalysts for the hydroxylation of various aromatic compounds to phenols, a process that concerns the activation of an inert C–H bond. Given the reactivity and broad substrate scope demonstrated herein, we anticipate that this study provide a new way for the direct hydroxylation of aromatic compounds. Although the Fe–Fe-bond-based oxygenation product, namely, the μ-O complex, which is postulated as the active intermediate for the hydroxylation, could not be obtained by the reaction of the [FeFe]-hydrogenase model complex with different oxidants,

DFT calculations and the catalytic activity towards hydroxylation suggest that it is capable of transferring an oxygen atom to the aromatic substrates. This study presents the catalytic application of these typical diiron carbonyl complexes. Although the yields of various phenols are not ideal, the selectivity is high. The diiron model complex with a more electron-donating ligand showed increased catalytic activity; on the basis of this insight, the design and development of diiron catalysts with higher catalytic activity and better substrate adaptability are ongoing in our laboratory.

Experimental Section

Materials and Methods: The syntheses of the model complexes and all other operations were carried out with a double-manifold Schlenk vacuum line under a N_2 atmosphere. Hexane, CH_2Cl_2, toluene, and CH_3CN were stored over molecular sieves under a N_2 atmosphere for 24 h prior to further purification. Hexane, CH_2Cl_2, and toluene were distilled under a N_2 atmosphere from sodium/benzophenone. CH_3CN was first stirred with anhydrous sodium sulfate at room temperature for 24 h and then distilled from NaH. The collected solvents were stored over molecular sieves under N_2 before use.

The following materials were of reagent grade and directly used as purchased from Guangfu Chemical Co.: H_2O_2 (30%), Me_3NO, PPh_3, AcOH, *m*-CPBA, benzene, and $AgNO_3$. 2,3-Butanedithiol, $Fe(CO)_5$, nBu_4NPF_6, and PhIO were purchased from Sigma–Aldrich.

Solution IR spectra were recorded with a Shimadzu NICOLET 380 spectrophotometer by using 0.1 mm KBr sealed cells. ^1H NMR spectra were recorded with a Bruker AVANCE III 400M spectrometer by using TMS as the internal standard in chloroform-d (deuterium content of 99.8 atom-%, contains 0.03% v/v TMS). Elemental analyses was carried out with a Heraeus CHN-O-Rapid fully automatic elemental analyzer with thermal-conductivity detection (TMT CHN-O).

For **1** and **1**-PPh_3, single-crystal X-ray diffraction data were recorded with a Rigaku MM-007 (rotating anode) diffractometer equipped with a Saturn 70CCD. Data were collected at 113 K by using a confocal monochromator with Mo-K_α radiation (λ = 0.71073 Å) in the ω–ϕ scanning mode. Data collection, reduction, and absorption correction were performed with the CRYSTALCLEAR program. The structures were solved by using direct methods and refined with the full-matrix least-squares technique by using the SHELXS-97[55] and SHELXL-97[56] programs. Hydrogen atoms were located by using the geometric method.

Data collection for **1**-O was performed at 298 K with a Rigaku-18 KW R-AXIS RAPID IP area detector by using graphite monochromated Mo-K_α radiation (λ = 0.71073 Å) in the oscillation scanning mode. For **1**-O, all calculations were performed with the SHELXTL-97 program package, and the structure was solved by using direct methods and refined by using full-matrix least-squares techniques against F^2. Data collection, reduction, and absorption correction were performed with the ABSCOR program.

CCDC-982213 (for **1**), -982214 (for **1**-PPh_3), and -982215 (for **1**-O) contain the supplementary crystallographic data for this paper, which can be obtained free of charge from The Cambridge Crystallographic Data Centre via www.ccdc.cam.ac.uk/data_request/cif.

Electrochemical measurements were carried out in CH_3CN solutions (ca. 2 mmol/L) with a CHI660B electrochemical workstation by using a three-electrode setup. Prior to use, the glassy-carbon (surface of 0.071 cm^2) working electrode was polished with an α-alumina polishing suspension and rinsed with CH_3CN. The counter electrode was a platinum wire. All potentials were recorded with respect to the Ag/Ag^+ reference electrode (0.01 M $AgNO_3$ and 0.1 mM nBu_4NPF_6 in CH_3CN), and the reported values are referenced against Fc/Fc^+ as a standard ($E_{1/2}$ = 0.00 V vs. Ag/Ag^+ in CH_3CN).

The phenol yield in the catalytic experiments was determined by using an external-standard method and was carried out with an Agilent 6890N gas chromatograph equipped with a capillary column (30 m × 0.25 mm × 0.25 μm) and a flame ionization detector.

DFT calculations were performed by using a hybrid functional [the three-parameter exchange functional of Becke (B3)[57] and the correlation functional of Lee, Yang, and Parr (LYP)[58] (B3LYP) as implemented in Gaussian 09].[59] The effective core potentials and the associated basis set of Hay and Wadt (LANL2DZ)[60,61] were used for the iron, sulfur, and phosphorus atoms. For iron atoms, the two outermost p functions were replaced by the re-optimized 4p functions as suggest by Couty and Hall.[62] For sulfur and phosphorus atoms, the basis set was augmented by the d polarization function of Höllwarth et al.[63] All carbon, oxygen, and hydrogen atoms were represented by using the double-valence ξ-basis (D95) of Dunning.[64] The geometries of all oxygenated isomers and non-oxygenated precursors were fully optimized and confirmed as minima by analytical frequency calculations at the same levels.

[(μ-dmedt){Fe(CO)$_3$}$_2$] (1): A solution of 2,3-butanedithiol (typically, 4.0 mL, 32 mmol) and $Fe(CO)_5$ (typically, 8.6 mL, 64 mmol) in toluene (50 mL) was heated at reflux under a N_2 atmosphere until a color change from green to red-brown was observed. After removal of the solvent by distillation, the products were purified by chromatography on successive silica columns with hexane as the eluent (4.2 g, 32.8%). Single crystals suitable for X-ray crystallographic analysis were obtained by slow diffusion of hexane into CH_2Cl_2 solution of **1**. FTIR (in hexane): $\tilde{\nu}$(CO) = 2075, 2035, 2006, 1990, 1981 cm^{-1}. ^1H NMR (400 MHz, $CDCl_3$): δ = 2.21 (m, 2 H, SC*H*), 1.33 (d, $^3J_{H,H}$ = 6.4 Hz, 6 H, CH_3C) ppm. $C_{10}H_8Fe_2O_6S_2$ (399.99): calcd. C 30.03, H 2.02, O 24.00; found C 30.10, H 2.05, O 23.94.

[(μ-dmedt){Fe(CO)$_3$}{Fe(CO)$_2$PPh$_3$}] (1-PPh$_3$): To a solution of **1** (0.20 g, 0.50 mmol) in CH_3CN (20 mL) under a N_2 atmosphere was added Me_3NO (1 equiv., 38 mg, 0.50 mmol) in CH_3CN (5 mL) to produce (μ-dmedt)[$Fe(CO)_3$] [$Fe(CO)_2NMe_3$] suggested by the IR monitor. To this solution, PPh_3 (1 equiv., 131 mg, 0.50 mmol) in CH_3CN (10 mL) was then added and subsequently heated at 80 °C for 5 h. After removal of CH_3CN in a vacuum, the products were purified by chromatography on successive silica columns monitored by IR spectroscopy. First, hexane was used as the eluent to remove **1**. Then, a mixture of hexane and CH_2Cl_2 (*V*/*V* = 1:1) was used as the eluent to collect **1**-PPh_3 (0.19 g, 60% yield). Crystals suitable for X-ray crystallographic analysis were obtained by slow diffusion of hexane into a CH_2Cl_2 solution of **1**-PPh_3. FTIR (in hexane): $\tilde{\nu}$(CO) = 2049, 1988, 1967, 1945 cm^{-1}. ^1H NMR (400 MHz, $CDCl_3$): δ = 7.62 (br., 9 H, Ph), 7.42 (br., 6 H, Ph), 1.95 (m, 2 H, SC*H*), 0.86 (d, $^3J_{H,H}$ = 6.8 Hz, 6 H, CH_3C) ppm. $C_{27}H_{23}Fe_2O_5PS_2$ (634.26): calcd. C 51.13, H 3.66, O 12.61; found C 51.20, H 3.62, O 12.52.

[(μ-dmest){Fe(CO)$_3$}$_2$] (1-O): To a solution of **1** (0.20 g, 0.50 mmol) in toluene (10 mL) was dropwise added under a N_2 atmosphere *m*-CPBA (1.5 equiv. in 10 mL of toluene). The mixture was stirred for 0.5 h at 20 °C and monitored by IR spectroscopy. Subsequently, gaseous ammonia was bubbled through the reaction mixture for

30 min to remove excess *m*-CPBA, and the *m*-chlorobenzoic acid by-product. After filtration and removal of the solvent, the resulting crude product (0.14 g, 67% yield) was dissolved in a minimal amount of MeOH and recrystallized at –30 °C to give the analytically pure product. Crystals suitable for X-ray analysis were grown from a CH_2Cl_2 solution layered with hexane. FTIR (in hexane): $\tilde{\nu}$(CO): 2082, 2043, 2020, 1997, 1988 cm^{-1}. ^1H NMR (400 MHz, $CDCl_3$): δ = 3.20 (m, 1 H, SC*H*), 2.10 (m, 1 H, SC*H*), 1.61 (d, $^3J_{H,H}$ = 6.4 Hz, 3 H, CH_3C), 1.39 (d, $^3J_{H,H}$ = 6.4 Hz, 3 H, CH_3C) ppm. $C_{10}H_8Fe_2O_7S_2$ (415.99): calcd. C 28.87, H 1.94, O 26.92; found C 28.79, H 2.02, O 26.83.

Hydroxylation of benzene and other aromatic substrates with H_2O_2 was carried out in a 25 mL round-bottomed flask equipped with a reflux condenser and a magnetic stirrer. In a typical reaction, the model complex **1** was dissolved in CH_3CN. After the mixture was heated to the desired temperature, benzene or other substrates were added to the mixture. Finally, a certain amount of H_2O_2 was added to initiate the hydroxylation, and the mixture was stirred for several hours. All the experiments were carried out at ambient pressure.

Acknowledgments

This work was supported by the National Natural Science Foundation of China (NSFC) (grant numbers 21103121, 21276187, 21236001), the Research Fund for the Doctoral Program of Higher Education of China (grant number 20110032120011), and the Tianjin Municipal Natural Science Foundation (grant number 13JCQNJC05800).

[1] O. Shoji, T. Kunimatsu, N. Kawakami, Y. Watanabe, *Angew. Chem. Int. Ed.* **2013**, *52*, 6606–6610.
[2] Z. Long, Y. Zhou, G. Chen, P. Zhao, J. Wang, *Chem. Eng. J.* **2014**, *239*, 19–25.
[3] R. Navarro, S. Lopez-Pedrajas, D. Luna, J. M. Marinas, F. M. Bautista, *Appl. Catal. A* **2014**, *474*, 272–279.
[4] S. Niwa, M. Eswaramoorthy, J. Nair, A. Raj, N. Itoh, H. Shoji, T. Namba, F. Mizukami, *Science* **2002**, *295*, 105–107.
[5] X. Chen, J. Zhang, X. Fu, M. Antonietti, X. Wang, *J. Am. Chem. Soc.* **2009**, *131*, 11658–11659.
[6] V. M. Zakoshansky, *Petroleum Chemistry* **2007**, *47*, 273–284.
[7] L. Chen, Y. Xiang, T. Feng, *Appl. Organomet. Chem.* **2012**, *26*, 108–113.
[8] Y. Li, H. Xia, F. Fan, Z. Feng, R. A. van Santen, E. J. M. Hensen, C. Li, *Chem. Commun.* **2008**, 774–776.
[9] S. Yang, G. Liang, A. Gu, H. Mao, *Ind. Eng. Chem. Res.* **2012**, *51*, 15593–15600.
[10] C. Walling, R. A. Johnson, *J. Am. Chem. Soc.* **1975**, *97*, 363–367.
[11] C. L. Sun, B. J. Li, Z. J. Shi, *Chem. Rev.* **2011**, *111*, 1293–1314.
[12] C. Bolm, J. Legros, J. L. Paih, L. Zani, *Chem. Rev.* **2004**, *104*, 6217–6254.
[13] C. M. Krest, E. L. Onderko, T. H. Yosca, J. C. Calixto, R. F. Karp, J. Livada, J. Rittle, M. T. Green, *J. Biol. Chem.* **2013**, *288*, 17074–17081.
[14] S. Friedle, E. Reisner, S. J. Lippard, *Chem. Soc. Rev.* **2010**, *39*, 2768–2779.
[15] M. Costas, M. P. Mehn, M. P. Jensen, L. Que Jr., *Chem. Rev.* **2004**, *104*, 939–986.
[16] M. A. Culpepper, G. E. Cutsail, B. M. Hoffman, A. C. Rosenzweig, *J. Am. Chem. Soc.* **2012**, *134*, 7640–7643.
[17] G. Gopakumar, P. Belanzoni, E. J. Baerends, *Inorg. Chem.* **2012**, *51*, 63–75.
[18] S. J. Lee, M. S. McCormick, S. J. Lippard, U. S. Cho, *Nature* **2013**, *494*, 380–384.
[19] H. Sun, M. Wang, F. Li, P. Li, Z. Zhao, L. Sun, *Appl. Organomet. Chem.* **2008**, *22*, 573–576.
[20] W. Nam, *Acc. Chem. Res.* **2007**, *40*, 522–531.
[21] B. Meunier, S. P. de Visser, S. Shaik, *Chem. Rev.* **2004**, *104*, 3947–3980.
[22] T. Jiang, W. Wang, B. Han, *New J. Chem.* **2013**, *37*, 1654–1664.
[23] P. Borah, X. Ma, K. T. Nguyen, Y. Zhao, *Angew. Chem. Int. Ed.* **2012**, *51*, 7756–7761.
[24] F. Shi, L. Mu, P. Yu, J. Hu, L. Zhang, *J. Mol. Catal. A* **2014**, *391*, 66–73.
[25] C. Guo, W. Du, G. Chen, L. Shi, Q. Sun, *Catal. Commun.* **2013**, *37*, 19–22.
[26] R. Bal, M. Tada, T. Sasaki, Y. Iwasawa, *Angew. Chem. Int. Ed.* **2006**, *45*, 448–452; *Angew. Chem.* **2006**, *118*, 462.
[27] Y. Ichihashi, T. Taniguchi, H. Amano, T. Atsumi, S. Nishiyama, S. Tsuruya, *Top. Catal.* **2008**, *47*, 98–100.
[28] W. Lubitz, H. Ogata, O. Rüdiger, E. Reijerse, *Chem. Rev.* **2014**, *114*, 4081–4148.
[29] M. E. Carroll, B. E. Barton, T. B. Rauchfuss, P. J. Carroll, *J. Am. Chem. Soc.* **2012**, *134*, 18843–18852.
[30] R. D. Bethel, M. L. Singleton, M. Y. Darensbourg, *Angew. Chem. Int. Ed.* **2010**, *49*, 8567–8569.
[31] C. Tard, C. J. Pickett, *Chem. Rev.* **2009**, *109*, 2245–2274.
[32] J. M. Camara, T. B. Rauchfuss, *J. Am. Chem. Soc.* **2011**, *133*, 8098–8101.
[33] J. M. Camara, T. B. Rauchfuss, *Nat. Chem.* **2012**, *4*, 26–30.
[34] T. Liu, B. Li, M. L. Singleton, M. B. Hall, M. Y. Darensbourg, *J. Am. Chem. Soc.* **2009**, *131*, 8296–8307.
[35] J. Messelhäuser, K. U. Gutensohn, I.-P. Lorenz, W. Hiller, *J. Organomet. Chem.* **1987**, *321*, 377–388.
[36] E. Y. Tshuva, S. J. Lippard, *Chem. Rev.* **2004**, *104*, 987–1012.
[37] D. Lee, S. J. Lippard, *Inorg. Chem.* **2002**, *41*, 2704–2719.
[38] M.-H. Baik, M. Newcomb, R. A. Friesner, S. J. Lippard, *Chem. Rev.* **2003**, *103*, 2385–2419.
[39] C. E. Tinberg, S. J. Lippard, *Acc. Chem. Res.* **2011**, *44*, 280–288.
[40] A. I. Stewart, I. P. Clark, M. Towrie, S. K. Ibrahim, A. W. Parker, C. J. Pickett, N. T. Hunt, *J. Phys. Chem. B* **2008**, *112*, 10023–10032.
[41] S. Munery, J.-F. Capon, L. D. Gioia, C. Elleouet, C. Greco, F. Y. Pétillon, P. Schollhammer, J. Talarmin, G. Zampella, *Chem. Eur. J.* **2013**, *19*, 15458–15461.
[42] F. Quentel, G. Passard, F. Gloaguen, *Chem. Eur. J.* **2012**, *18*, 13473–13479.
[43] C. M. Thomas, O. Rüdiger, T. Liu, C. E. Carson, M. B. Hall, M. Y. Darensbourg, *Organometallics* **2007**, *26*, 3976–3984.
[44] L. C. Song, C. G. Li, J. H. Ge, Z. Y. Yang, H. T. Wang, J. Zhang, Q. M. Hu, *J. Inorg. Biochem.* **2008**, *102*, 1973–1979.
[45] R. Mejia-Rodriguez, D. Chong, J. H. Reibenspies, M. P. Soriaga, M. Y. Darensbourg, *J. Am. Chem. Soc.* **2004**, *126*, 12004–12014.
[46] P. Li, M. Wang, C. He, G. Li, X. Liu, C. Chen, B. Åkermark, L. Sun, *Eur. J. Inorg. Chem.* **2005**, 2506–2513.
[47] D. Chong, I. P. Georgakaki, R. Mejia-Rodriguez, J. Sanabria-Chinchilla, M. P. Soriaga, M. Y. Darensbourg, *Dalton Trans.* **2003**, 4158–4163.
[48] I. P. Georgakaki, M. L. Miller, M. Y. Darensbourg, *Inorg. Chem.* **2003**, *42*, 2489–2494.
[49] X. Zhao, I. P. Georgakaki, M. L. Miller, R. Mejia-Rodriguez, C.-Y. Chiang, M. Y. Darensbourg, *Inorg. Chem.* **2002**, *41*, 3917–3928.
[50] W. Dong, M. Wang, T. Liu, X. Liu, K. Jin, L. Sun, *J. Inorg. Biochem.* **2007**, *101*, 506–513.
[51] J. Windhager, R. A. Seidel, U.-P. Apfel, H. Görls, G. Linti, W. Weigand, *Chem. Biodiversity* **2008**, *5*, 2023–2041.
[52] M. Y. Darensbourg, W. Weigand, *Eur. J. Inorg. Chem.* **2011**, 994–1004.
[53] J. Windhager, M. Rudolph, S. Bräutigam, H. Görls, W. Weigand, *Eur. J. Inorg. Chem.* **2007**, 2748–2760.
[54] T. Vannelli, A. B. Hooper, *Biochemistry* **1995**, *34*, 11743–11749.
[55] G. Sheldrick, *SHELXS-97*, *Program for Crystal Structure Solution*, University of Göttingen, Germany, **1997**.

[56] G. Sheldrick, *SHELXL-97*, *Program for Crystal Structure Refinement*, University of Göttingen, Germany, **1997**.
[57] A. D. Becke, *J. Chem. Phys.* **1993**, *98*, 5648–5652.
[58] C. Lee, W. Yang, R. G. Parr, *Phys. Rev. B* **1988**, *37*, 785–789.
[59] M. J. Frisch, G. W. Trucks, H. B. Schlegel, G. E. Scuseria, M. A. Robb, J. R. Cheeseman, G. Scalmani, V. Barone, B. Mennucci, G. A. Petersson, H. Nakatsuji, M. Caricato, X. Li, H. P. Hratchian, A. F. Izmaylov, J. Bloino, G. Zheng, J. L. Sonnenberg, M. Hada, M. Ehara, K. Toyota, R. Fukuda, J. Hasegawa, M. Ishida, T. Nakajima, Y. Honda, O. Kitao, H. Nakai, T. Vreven, J. A. Montgomery Jr., J. E. Peralta, F. Ogliaro, M. Bearpark, J. J. Heyd, E. Brothers, K. N. Kudin, V. N. Staroverov, R. Kobayashi, J. Normand, K. Raghavachari, A. Rendell, J. C. Burant, S. S. Iyengar, J. Tomasi, M. Cossi, N. Rega, J. M. Millam, M. Klene, J. E. Knox, J. B. Cross, V. Bakken, C. Adamo, J. Jaramillo, R. Gomperts, R. E. Stratmann, O. Yazyev, A. J. Austin, R. Cammi, C. Pomelli, J. W. Ochterski, R. L. Martin, K. Morokuma, V. G. Zakrzewski, G. A. Voth, P. Salvador, J. J. Dannenberg, S. Dapprich, A. D. Daniels, O. Farkas, J. B. Foresman, J. V. Ortiz, J. Cioslowski, D. J. Fox, *Gaussian 09*, revision D.01, Gaussian, Inc., Wallingford CT, **2009**.
[60] P. J. Hay, W. R. Wadt, *J. Chem. Phys.* **1985**, *82*, 270–283.
[61] W. R. Wadt, P. J. Hay, *J. Chem. Phys.* **1985**, *82*, 284–298.
[62] M. Couty, M. B. Hall, *J. Comput. Chem.* **1996**, *17*, 1359–1370.
[63] A. Höllwarth, M. Böhme, S. Dapprich, A. W. Ehlers, A. Gobbi, V. Jonas, K. F. Köhler, R. Stegmann, A. Veldkamp, G. Frenking, *Chem. Phys. Lett.* **1993**, *208*, 237–240.
[64] J. T. H. Dunning, *J. Chem. Phys.* **1970**, *53*, 2823–2833.

Received: September 25, 2014
Published Online: ■

Bio-Inspired Diiron Complexes

Keywords: Diiron complex / Hydroxylation / Aromatic compounds / O–O activation / Density functional calculations

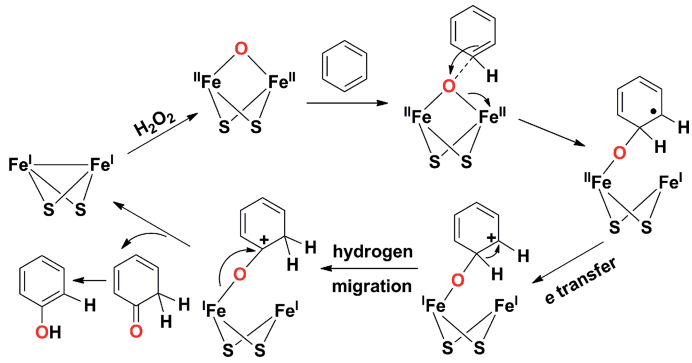

Three Fe^{I}–Fe^{I} organometallic complexes were synthesized and used as highly selective catalysts for the direct hydroxylation of aromatic compounds to phenols, forming Fe^{II}–μ-O–Fe^{II} intermediates as the active oxygen-transfer species.

